CIMAC CONGRESS 25
ZURICH, MAY 19 – 23, 2025

2025 | 418

Genetic algorithm-assisted performance prediction of an MW-scale ammonia-diesel dual-fuel engine

Dual Fuel / Gas / Diesel

Yan Zhang, University of Birmingham

Dawei Wu, University of Birmingham
Ebrahim Nadimi, University of Birmingham
Yuqi Zhang, University of Birmingham
Athanasios Tsolakis, University of Birmingham

ABSTRACT

Ammonia (NH3) has emerged as a promising alternative marine fuel, offering higher energy storage density compared with hydrogen for deep-sea vessels. However, the lack of reliable experimental data and validated models for large-scale marine engines (over one MW) poses significant challenges for researchers and asset owners. This study addresses this gap by developing a parameterization method using a multi-objective optimization approach based on a genetic algorithm (GA) for predicting the performance of a retrofitted ammonia-diesel dual-fuel engine. This method extracts combustion profiles from experiments on a small ammonia-diesel compression ignition engine, facilitating their application in a scaled-up dual-fuel engine model for performance prediction.

Experimental work on the small diesel engine, later modified to a dual-fuel engine, explored various dual-fuel ratios and in-cylinder injection timings, generating comprehensive data on combustion characteristics under different operating conditions. The proposed GA-assisted parameterization method was verified under pure diesel conditions, demonstrating accuracy within a 5% error margin for in-cylinder pressure and characterizing combustion phases using a multi-Wiebe function.

The same method was applied to the dual-fuel engine, generating a credible model in GT-Power through parameterization. It revealed that with a 60% NH3 heat fraction, the heat release rate (HRR) curve broadened and slightly decreased in magnitude compared with lower NH3 fractions. This is attributed to the higher presence of liquid NH3, which requires additional heat for vaporization in the cylinder, leading to a distinct two-stage combustion process before the HRR peak.

With a better understanding of dual-fuel combustion characteristics from the small engine, the multi-Wiebe function for ammonia combustion was further applied in the development and simulation of an MW-scale marine diesel engine. The simulation results indicated that increasing the NH3 heat fraction in the dual-fuel mix significantly lowers the combustion temperature and pressure in a large marine engine. The predicted performance characteristics of the MW-scale dual-fuel engine, such as power and speed, align well with findings from the literature on both small and large dual-fuel engines, compared with baseline diesel engines, validating the model's credibility and scalability.

In summary, this study provides a novel and validated approach for modeling ammonia-diesel dual-fuel combustion in MW-scale marine engines. The findings underscore the feasibility and benefits of using ammonia as a marine fuel, offering a pathway towards more sustainable and efficient marine propulsion systems.

1 INTRODUCTION

In the marine industry, which accounts for 11% of greenhouse gas emissions in the transportation sector, internal combustion engines serve as the primary power source for propulsion [1]. Developing zero-carbon technologies to reduce greenhouse gas emissions in the marine shipping sector is crucial. Ammonia has been studied as an alternative fuel to fossil fuels [2]. With its high hydrogen content, ammonia could act as a hydrogen carrier to support zero-carbon goals in the era of carbon peaking and carbon neutrality [3]. For deep-sea vessels, ammonia Compression Ignition (CI) engine offers an efficient solution for the decarbonization of the marine industry [4].

Numerous studies have been conducted on ammonia CI engines. In the experiment domain, most studies have focused on ammonia engines with displacements of up to 10L, as summarised in Table 1. Existing studies explored the effects of injection methods, including injection pressure and timing, as well as the ammonia energy ratio, on engine performance and emissions. These studies provide valuable insights and potential solutions for the development of ammonia CI engines. In the marine industry, ammonia CI engines with high-displacement and multi-cylinder are essential for development and practical application. Addressing the challenges of designing and testing large ammonia CI engines with displacements exceeding 30L, simulation studies play a crucial role in advancing progress in this field.

Table 1 Experimental studies of ammonia-diesel CI engines (PFI: Port Fuel Injection, DI: Direct Injection)

Reference	Displacement	Injection method	Main studied parameters
Bjorgen et al. [5]	0.3468L	ammonia: DI diesel: DI	ammonia injection timing: -20→-10 CAD aTDC, diesel injection timing: -15 CAD aTDC ammonia injection timing = diesel injection timing: -20→-10 CAD aTDC ammonia energy ratio: 40%→60%, diesel mass fixed
Jin et al. [6]	9.5L	ammonia: PFI diesel: DI	ammonia energy ratio: 0 → 90%
Nadimi et al. [7]	0.406L	ammonia: PFI diesel: DI	ammonia energy ratio: 0 → 84.16%
Hossein et al. [8]	2.44 L	ammonia: PFI diesel: DI	ammonia energy ratio: 30% → 70%
Elbanna et al. [9]	1.85L	ammonia: PFI diesel: DI	ammonia energy ratio: 0 → 30% diesel injection timing: -12→-4 CAD aTDC
Shin et al. [10]	2.44L	ammonia: DI diesel: DI	ammonia energy ratio: 90%→99% ammonia injection timing: -40→-3 CAD aTDC, diesel injection timing: -15 CAD aTDC ammonia injection timing: -7 CAD aTDC, diesel injection timing: -25→-10 CAD aTDC
Wang et al. [11]	3.26L	ammonia: PFI diesel: DI	main injection timing: -12→-4 CAD aTDC pre-injection timing: -36→-24 CAD aTDC pre-injection quantity: 1.2→2.8mg diesel injection pressure: 100→140MPa
Liu et al. [12]	3.26L	ammonia: PFI diesel: DI	ammonia energy ratio: 0→60% diesel injection pressure: 100→140MPa diesel injection timing: -12→-4 CAD aTDC
Li et al. [13]	0.721 L	ammonia: DI diesel: DI	ammonia energy ratio: 90%, 80%, 70% injection pressure: high and low
Kishore et al. [14]	0.909L	ammonia: PFI diesel: DI	ammonia energy ratio: 0→46.88%

Following experimental studies, numerous simulation studies have been employed to support the research and development of ammonia CI engines. Computational Fluid Dynamics (CFD) models have been used to design and analysis the combustion process of ammonia CI engines [15]. Working as a 3-D (3-Dimension) model, CFD model is complex and focuses on simulating the processes within the cylinder. Research and analysis of multi-cylinder ammonia CI engines require a 1-D (1-Dimension) model, which is also well-suited for powertrain-level studies [16]. In the 1-D engine model, incorporating a 0-D (0-Dimension) combustion model is essential for ensuring simulation accuracy. The 0-D model emphasizes time-dependent changes in thermodynamic states, rather than the spatial distribution of physical quantities such as temperature, pressure, and velocity [17]. This approach is commonly employed to predict engine performance and behaviour.

Among 0-D combustion models, the Wiebe combustion model is the most widely utilized for

simulating combustion processes within the cylinder [18]. As shown in

Table 2, numerous studies have explored the application of the Wiebe combustion model in engine simulations, highlighting its potential for accurate predictions and simulations in the context of alternative fuel engines and dual-fuel engines. To improve the accuracy of in-cylinder combustion simulations, double and triple Wiebe combustion models, along with optimization methods, have been developed to refine the calculation of Wiebe parameters.

Table 2 Studies related to Wiebe combustion model

Reference	Engine type	Fuel type	Combustion model	Notes
Rajendra et al. [19]	4-stroke CI engine	Biodiesel: DI	Single-Wiebe combustion model	A comprehensive cycle simulation program for engine by "C" language
Kim et al. [20]	4-stroke SI engine	liquefied petroleum gas: premixed	Single-Wiebe combustion model	Simulation model for engine by MATLAB/Simulink
Maroteaux et al. [21, 22]	4-stroke SI engine	Diesel: DI	Double-Wiebe combustion model	Simulation model for engine by MATLAB/Simulink, HIL
Ngayihi et al. [23]	4-stroke SI engine	Neem methyl esther biodiesel: DI	Double-Wiebe combustion model	MATLAB code
Bondarenko et al. [24]	2-stroke CI engine	Diesel: DI	Single-Wiebe combustion model	Digital twin model of the powertrain
de Faria et al. [25]	4-stroke SI engine	Biogas: premixed	Single-Wiebe combustion model	Wolfram Mathematica 7 was used for the simulation procedure
Sapra et al. [26]	4-stroke SI engine	Hydrogen and Natural gas: premixed	Double-Wiebe combustion model	0D/1D engine model in GT-ISE
Aklouche et al. [27]	4-stroke CI engine	Diesel: DI Biogas or natural gas: premixed	Double-Wiebe combustion model	The least squares method was used for the calculation of Wiebe parameters
Tipanluisa [28]	4-stroke CI engine	diesel/n-butanol blends	Triple-Wiebe combustion model	The partial least square approximation technique for multiple variables was utilized to fit the Wiebe parameters
Liu et al.[29]	4-stroke CI engine	Natural gas: premixed	Triple-Wiebe combustion model	The least-squares method was employed for the calculation process.
Loganathan et al. [30]	4-stroke CI engine	Dimethyl Ether: DI	Double-Wiebe combustion model	Oxygenate correction factor and Load correction factor were used for the prediction of Wiebe parameters
Salvi et al. [31]	4-stroke SI engine	Hydrogen: premixed	Single-Wiebe combustion model	The computer programme was developed in MATLAB, EGR
Mishra et al. [32]	4-stroke CI engine	Diesel: DI Gasoline: PFI	Double-Wiebe combustion model	Correlative model using random forest machine learning was used for the construction of Wiebe parameters

To address the challenges associated with conducting experiments during the design and development process of large bore ammonia CI engines, and the lack of a 0-D combustion model for 1-D simulations of such marine engines, this study focuses on developing a Multi-Wiebe Combustion (MWC) model for a large Ammonia-Diesel Compression Ignition (ADCI) engine. Multi-objective optimization, supported by Non-dominated Sorting Genetic Algorithm II (NSGA-II), is utilized to facilitate the calculation and parameterization of the MWC model. Additionally, a GT-Power simulation model is developed to predict and analyse the combustion performance of the large ADCI engine. The optimization and simulation results offer valuable insights into the interaction between ammonia and diesel fuels within the engine, enhancing the development of large ADCI engine.

2 METHODOLOGY

2.1 Multiple Wiebe Combustion Model

In diesel CI engines, the combustion process can be divided into three phases: premixed combustion phase (PCP), main combustion phase (MCP) and tail combustion phase (TCP) [29, 33]. In the ADCI engine, two types of fuel are burned within the cylinder. Diesel combustion occurs in three distinct phases due to direct injection, while ammonia combustion follows two phases due to port injection. Therefore, five Wiebe functions are used for the ADCI engine as follows [28]:

$$\theta_{\mathrm{SoC\_a}} = \theta_{\mathrm{SOI\_a}} + t_{\mathrm{ID\_a}}$$
$$\theta_{\mathrm{SoC\_d}} = \theta_{\mathrm{SOI\_d}} + t_{\mathrm{ID\_d}} \quad (1)$$

$$P_{\mathrm{M\_a}} = 1 - P_{\mathrm{T\_a}}$$
$$P_{\mathrm{M\_d}} = 1 - P_{\mathrm{P\_d}} - P_{\mathrm{T\_d}} \quad (2)$$

$$p_{\mathrm{M\_a}}(\theta) = \alpha_{\mathrm{a}} \cdot P_{\mathrm{M\_a}} \cdot \left(1 - \mathrm{e}^{-C_{\mathrm{M\_a}} \cdot \left(\theta - \theta_{\mathrm{SoC\_a}}\right)^{\left(E_{\mathrm{M\_a}}+1\right)}}\right)$$
$$p_{\mathrm{T\_a}}(\theta) = \alpha_{\mathrm{a}} \cdot P_{\mathrm{T\_a}} \cdot \left(1 - \mathrm{e}^{-C_{\mathrm{T\_a}} \cdot \left(\theta - \theta_{\mathrm{SoC\_a}}\right)^{\left(E_{\mathrm{T\_a}}+1\right)}}\right) \quad (3)$$

$$p_{\mathrm{P\_d}}(\theta) = \alpha_{\mathrm{d}} \cdot P_{\mathrm{P\_d}} \cdot \left(1 - \mathrm{e}^{-C_{\mathrm{P\_d}} \cdot \left(\theta - \theta_{\mathrm{SoC\_d}}\right)^{\left(E_{\mathrm{PCP\_d}}+1\right)}}\right)$$
$$p_{\mathrm{M\_d}}(\theta) = \alpha_{\mathrm{d}} \cdot P_{\mathrm{M\_d}} \cdot \left(1 - \mathrm{e}^{-C_{\mathrm{M\_d}} \cdot \left(\theta - \theta_{\mathrm{SoC\_d}}\right)^{\left(E_{\mathrm{M\_d}}+1\right)}}\right) \quad (4)$$
$$p_{\mathrm{T\_d}}(\theta) = \alpha_{\mathrm{d}} \cdot P_{\mathrm{T\_d}} \cdot \left(1 - \mathrm{e}^{-C_{\mathrm{T\_d}} \cdot \left(\theta - \theta_{\mathrm{SoC\_d}}\right)^{\left(E_{\mathrm{T\_d}}+1\right)}}\right)$$

where, a refers to ammonia; d refers to diesel; p_{P}, p_{M} and p_{T} are the proportion of fuel burned in the PCP, MCP and TCP, respectively; α is the fraction of fuel burned or combustion efficiency; C_{P}, C_{M} and C_{T} are the Wiebe constant of PCP, MCP and TCP, respectively; E_{P}, E_{M} and E_{T} are the combustion exponent of PCP, MCP and TCP, respectively; P_{P}, P_{M} and P_{T} are the integration of the proportion of fuel burned in PCP, MCP and TCP, respectively; θ_{SOC} is the Start of Combustion (SOC); θ_{SOI} is the Start of Injection (SOI); t_{ID} is the Ignition Delay (ID).

The calculation of the Wiebe constant in the equation (3) and (4) is as follows:

$$C_{\mathrm{BM}} = -\ln\left(1 - P_{\mathrm{BM}}\right)$$
$$C_{\mathrm{BS}} = -\ln\left(1 - P_{\mathrm{BS}}\right) \quad (5)$$
$$C_{\mathrm{BE}} = -\ln\left(1 - P_{\mathrm{BE}}\right)$$

$$C_{\mathrm{M\_a}} = \left(\frac{D_{\mathrm{M\_a}}}{C_{\mathrm{BE}}^{\frac{1}{E_{\mathrm{M\_a}}+1}} - C_{\mathrm{BS}}^{\frac{1}{E_{\mathrm{M\_a}}+1}}}\right)^{-\left(E_{\mathrm{M\_a}}+1\right)}$$
$$C_{\mathrm{T\_a}} = \left(\frac{D_{\mathrm{T\_a}}}{C_{\mathrm{BE}}^{\frac{1}{E_{\mathrm{T\_a}}+1}} - C_{\mathrm{BS}}^{\frac{1}{E_{\mathrm{T\_a}}+1}}}\right)^{-\left(E_{\mathrm{T\_a}}+1\right)} \quad (6)$$

$$C_{\mathrm{P\_d}} = \left(\frac{D_{\mathrm{P\_d}}}{C_{\mathrm{BE}}^{\frac{1}{E_{\mathrm{P\_d}}+1}} - C_{\mathrm{BS}}^{\frac{1}{E_{\mathrm{P\_d}}+1}}}\right)^{-\left(E_{\mathrm{P\_d}}+1\right)}$$
$$C_{\mathrm{M\_d}} = \left(\frac{D_{\mathrm{M\_d}}}{C_{\mathrm{BE}}^{\frac{1}{E_{\mathrm{M\_d}}+1}} - C_{\mathrm{BS}}^{\frac{1}{E_{\mathrm{M\_d}}+1}}}\right)^{-\left(E_{\mathrm{M\_d}}+1\right)} \quad (7)$$
$$C_{\mathrm{T\_d}} = \left(\frac{D_{\mathrm{T\_d}}}{C_{\mathrm{BE}}^{\frac{1}{E_{\mathrm{T\_d}}+1}} - C_{\mathrm{BS}}^{\frac{1}{E_{\mathrm{T\_d}}+1}}}\right)^{-\left(E_{\mathrm{T\_d}}+1\right)}$$

where, D_{P}, D_{M} and D_{T} are the combustion duration of PCP, MCP and TCP, respectively; C_{BE} is the burned end constant; C_{BS} is the burned start constant; C_{BM} is the burned mid-point constant; P_{BM} is the burned fuel percentage at burned mid-point, and its value is always being set to 0.5; P_{BS} is the burned fuel percentage at duration start, and its value is always being set to 0.1; P_{BE} is the burned fuel percentage at duration end, and its value is always being set to 0.9.

Therefore, in ADCI engines, the total proportion of fuel burned throughout the entire combustion process is as follows:

$$p_{\mathrm{total}}(\theta) = \gamma_{\mathrm{a}} \cdot p_{\mathrm{a}}(\theta) + \gamma_{\mathrm{d}} \cdot p_{\mathrm{d}}(\theta)$$
$$p_{\mathrm{a}}(\theta) = p_{\mathrm{M\_a}}(\theta) + p_{\mathrm{T\_a}}(\theta) \quad (8)$$
$$p_{\mathrm{d}}(\theta) = p_{\mathrm{P\_d}}(\theta) + p_{\mathrm{M\_d}}(\theta) + p_{\mathrm{T\_d}}(\theta)$$

where, θ is the instantaneous crank angle; p_{total} is the proportion of total fuel burned; p_{a} and p_{d} are the proportion of ammonia and diesel burned, respectively; γ_{a} and γ_{d} are the proportion of ammonia and diesel in the mixture, respectively.

2.2 Optimization Method

As shown in Section 2.1, several parameters need to be calculated for the MWC model. They are the proportion of each combustion phase for each fuel ($P_{\mathrm{M\_a}}$, $P_{\mathrm{T\_a}}$, $P_{\mathrm{P\_d}}$, $P_{\mathrm{M\_d}}$, $P_{\mathrm{T\_d}}$), the burning duration of each combustion phase for each fuel ($D_{\mathrm{M\_a}}$, $D_{\mathrm{T\_a}}$, $D_{\mathrm{P\_d}}$, $D_{\mathrm{M\_d}}$, $D_{\mathrm{T\_d}}$), the exponent of each combustion phase for each fuel ($E_{\mathrm{M\_a}}$, $E_{\mathrm{T\_a}}$, $E_{\mathrm{P\_d}}$, $E_{\mathrm{M\_d}}$, $E_{\mathrm{T\_d}}$), and the ignition delay of each fuel ($t_{\mathrm{ID\_a}}$, $t_{\mathrm{ID\_d}}$). As shown in the equation (2), $P_{\mathrm{M\_a}}$ and $P_{\mathrm{M\_d}}$ can be calculated indirectly. Therefore, there are fifteen parameters to be determined in the MWC model for ADCI engines. To accelerate the calculation speed and improve the accuracy of the results, an optimization method is developed in this section.

2.2.1 Objective Function

To achieve accurate results in the optimization process, a suitable objective function must be selected as the optimization target. The goal of the calculations of the MWC model is to closely align with experimental data. Therefore, the error between the fitting results and experimental results should be minimized.

Residual Sum of Squares (RSS) measures the sum of squares differences between the fitting results and experimental results. The value of RSS should be minimized to achieve close alignment between the fitting results and experimental results. The function of RSS is given as follows:

$$e_{\mathrm{RSS}} = \sum \left(X_i - Y_i \right)^2 \tag{9}$$

where, e_{Rss} is the value of RSS; X_i and Y_i are the individual data point of variable X and variable Y, respectively.

When using RSS as the objective function, it should be defined as follows:

$$\begin{aligned} f_1 &= \min\left(e_{\mathrm{RSS}}\right) \\ &= \min\left(\sum \left(r_{\mathrm{fit}}(\theta) - r_{\mathrm{exp}}(\theta) \right)^2 \right) \end{aligned} \tag{10}$$

where, r_{fit} and r_{exp} are the Rate of Fuel Burned Proportion (FBPR) of fitting result and experimental result, respectively.

The R-square (R^2) is a popular and efficient metric for evaluating how well the model fits the experimental data. The value range of R^2 is from 0 to 1, where a value of 1 indicates a perfect fit, and a value of 0 means the model has no correlation with the experimental data. The function is given as follows:

$$e_{\mathrm{R2}} = 1 - \frac{\sum \left(X_i - Y_i \right)^2}{\sum \left(X_i - \overline{X} \right)^2} \tag{11}$$

where, e_{R2} is the value of R^2; $\overline{X}$ is the means of variable X.

When using R^2 as the objective function, it should be defined as follows:

$$\begin{aligned} f_2 &= \min\left(1 - e_{\mathrm{R2}}\right) \\ &= \min\left(1 - \frac{1 - \sum \left(r_{\mathrm{fit}}(\theta) - r_{\mathrm{exp}}(\theta) \right)^2}{\sum \left(r_{\mathrm{fit}}(\theta) - \bar{r}_{\mathrm{fit}} \right)^2} \right) \end{aligned} \tag{12}$$

where, $\bar{r}_{\mathrm{fit}}$ is the means of the FBPR of fitting results.

Pearson Correlation Coefficient (PCC) is useful for measuring the linear relationship between the fitting results and experimental data. The value range of PCC is from -1 to 1, where 1 indicates a strong positive linear relationship, 0 indicates no linear relationship, and -1 indicates a strong negative linear relationship. The function of PCC is given as follows:

$$e_{\mathrm{PCC}} = \frac{\sum \left(\left(X_i + \overline{X} \right) \cdot \left(Y_i + \overline{Y} \right) \right)}{\sqrt{\sum \left(X_i + \overline{X} \right)^2 \cdot \sum \left((Y_i + \overline{Y}) \right)^2}} \tag{13}$$

where, e_{PCC} is the value of PCC; $\overline{Y}$ is the means of variable Y.

When using PCC as the objective function, it should be defined as follows:

$$\begin{aligned} f_3 &= \min\left(1 - e_{\mathrm{PCC}}\right) \\ &= \min\left(1 - \frac{\sum \left(\left(r_{\mathrm{fit}}(\theta) + \bar{r}_{\mathrm{fit}} \right) \cdot \left(r_{\mathrm{exp}}(\theta) + \bar{r}_{\mathrm{exp}} \right) \right)}{\sqrt{\sum \left(r_{\mathrm{fit}}(\theta) + \bar{r}_{\mathrm{fit}} \right)^2 \cdot \sum \left(r_{\mathrm{exp}}(\theta) + \bar{r}_{\mathrm{exp}} \right)^2}} \right) \end{aligned} \tag{14}$$

where $\bar{r}_{\mathrm{exp}}$ is the means of the FBPR of experimental results.

RSS, R^2 and PCC assess how well the fitting results align with the experimental data from different perspectives. Therefore, the objective function f_1, f_2 and f_3 serve as multiple objective functions in the optimization process of this study. To evaluate the convergence of the optimization process and assist in selecting the optimal solution, a comprehensive objective function is introduced. By assigning weights to each individual objective function, the final comprehensive objective function is formulated as follows:

$$F = \min\left(\sum_{n=1}^{N} w_n f_n \right) \tag{15}$$

where, w_n is the weight of the n^{th} objective function. N is the number of objective functions.

2.2.2 Constraint Conditions

During the combustion process, the amount of fuel burned should be limited to the quantity injected into the cylinder. The function representing this constraint is given as follows:

$$P_a(\theta) \le \mu_a(\theta)$$
$$P_d(\theta) \le \mu_d(\theta) \quad (16)$$

$$\mu_a(\theta) = \begin{cases} 0, \theta < \theta_{SOI\_a} \\ \int_{\theta_{SOI\_a}}^{\theta} S_a(\theta) d\theta, \theta_{SOI\_a} \le \theta < \theta_{EOI\_a} \\ 1, \theta \ge \theta_{EOI\_a} \end{cases}$$
$$\mu_d(\theta) = \begin{cases} 0, \theta < \theta_{SOI\_d} \\ \int_{\theta_{SOI\_d}}^{\theta} S_d(\theta) d\theta, \theta_{SOI\_d} \le \theta < \theta_{EOI\_d} \\ 1, \theta \ge \theta_{EOI\_d} \end{cases} \quad (17)$$

where, μ_a and μ_d are the normalized fuel content of ammonia and diesel, which have been injected into the cylinder, respectively; S_a and S_d are the normalized fuel injection rates of ammonia and diesel, respectively; θ_{EOI_a} and θ_{EOI_d} are the end of injection points of ammonia and diesel, respectively.

Based on the experimental data, the range of ignition timing for diesel can be predicted. Given the combustion characteristics of diesel and ammonia, the ignition time for ammonia should occur later than that of diesel. The function representing this constraint is shown as follows:

$$\theta_{SoC\_d} < \theta_{SoC\_a} \quad (18)$$

The range of exponent for each fuel in each combustion phase is between 0.3 and 2 [34]. The range of combustion duration and proportion for each fuel in each combustion phase are predicted based on the experimental data.

To achieve optimal fitting results, the Relative Error (RE) of key points should be kept within a low range. These key points include the maximum FBFR and the crank angle at which the maximum FBFR occurs. The function representing this constraint is given as follows:

$$\left|e_{RE\_rmax}\right| = \left|\frac{r_{max\_fit} - r_{max\_exp}}{r_{max\_exp}}\right| \in [0, 0.05]$$
$$\left|e_{RE\_\theta\_rmax}\right| = \left|\frac{\theta_{r\,max\_fit} - \theta_{r\,max\_exp}}{\theta_{r\,max\_exp}}\right| \in [0, 0.05] \quad (19)$$

where, r_{max_fit} and r_{max_exp} are the maximum FBPR of the fitting result and the experimental result, respectively; θ_{rmax_fit} and θ_{rmax_exp} is the crank angle at which the maximum FBPR occurs in the fitting result and experimental result, respectively; e_{RE_rmax} is the RE in the maximum FBPR; $e_{RE\_\theta\_rmax}$ is the RE in the crank angle at maximum FBPR.

2.2.3 Optimization Method – NSGA-II

To calculate the fifteen Wiebe parameters for the MWC model, NSGA-II is employed as the optimization algorithm. By using the fast non-dominated sorting algorithm, NSGA-II offers low complexity, rapid calculation speed, and improved converge quality. The optimization process can be terminated once the cutoff condition is met. The cutoff condition is specified as follows:

$$G \ge G_{max} \quad (20)$$

where, G is the number of generations; G_{max} is the maximum threshold of generations.

The optimization process, as shown in Figure 1, follows these steps: (i) The initial population is generated based on the input parameters and constraint conditions. (ii) The population is evaluated using the objective functions, sorted, feasibility assessed, and crowding distances calculated. (iii) A new generation is created through selection, crossover, mutation, and correction of infeasible solutions. (iv) The results are evaluated: If the cutoff condition is met, the final results are produced, and the optimization process concludes. If not, the process returns to step (ii) and continues.

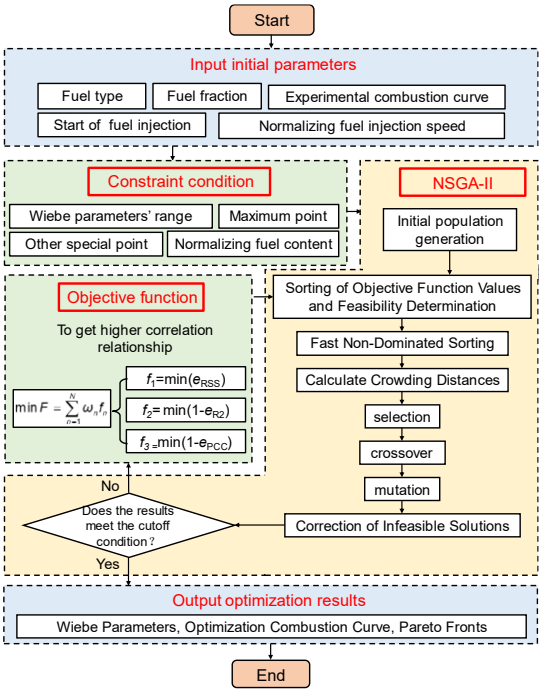

Figure 1 Diagram of the NSGA-II optimization process

2.3 Simulation Model

In this study, the Wärtsilä 32 engine serves as the base engine for analysis, with its specifications provided in Table 3. The experiment data used in this study is obtained from the reference [35]. To

validate the accuracy of the MWC model, which is computed using NSGA-II, and to simulate the performance of the multi-cylinder engine, a 1-D simulation model is developed in GT-Power.

For the fuel injection system, ammonia is introduced through a port injection system equipped with an 8-nozzle injector, each nozzle having a diameter of 0.2 mm, ensuring thoroughly mixing with air before combustion. Diesel is injected via a direct injection system to serve as the pilot fuel, operating at an injection pressure of 150 MPa.

Table 3 Engine specifications and basic operating conditions

	Parameter	Unit	Data
Engine specifications	Engine type		4-stroke
	Number of cylinders		6
	Compression ratio		16:1
	Bore/Stroke	mm	320/400
	Displacement volume	L/cyl	32.2
	Connecting rod length	mm	848
Operating parameters	Engine speed	rpm	750
	Injection pressure of diesel	MPa	150
	Intake temperature	℃	40
	Fuel temperature	℃	60

2.4 Case Setup

This study analyses various diesel injection timings at a high energy substitution rate to examine the interaction dynamics of ammonia in a large ADCI engine and its impact on engine performance. The goal is to accelerate the adoption of high ammonia substitution rates in large ADCI engines for the marine industry. The cases setup is provided in Table 4 [35].

Table 4 Cases setup. φ_a is the equivalence ratio of the ammonia/air mixture; $InjD_d$ is the injection duration of diesel.

	Unit	Case 1	Case 2	Case 3
β_a	%	91.85	91.85	91.85
φ_a		0.58	0.58	0.58
m_a	g/cycle	3.276	3.276	3.276
m_d	g/cycle	0.125	0.125	0.125
θ_{SOI_a}	CAD aTDC	-350	-350	-350
θ_{SOI_d}	CAD aTDC	-10	-15	-20
$InjD_d$	CAD	8.64	8.64	8.64

The energy share ratio of each fuel in a mixed-fuel scenario could be calculated as follows:

$$\beta_d = \frac{m_d \cdot \lambda_d}{m_d \cdot \lambda_d + m_a \cdot \lambda_a}$$
$$\beta_a = \frac{m_a \cdot \lambda_a}{m_d \cdot \lambda_d + m_a \cdot \lambda_a} \quad (21)$$

where, β_d and β_a are the energy share ratio of diesel and ammonia, respectively; m_d and m_a are the mass of diesel and ammonia, respectively; λ_d and λ_a are the lower heating value of diesel and ammonia, respectively.

3 RESULTS AND ANALYSIS

3.1 Validation

3.1.1 Pareto Front and Convergence

In the optimization process, as shown in Figure 2, the Pareto nondominated solution set covers the solution space, demonstrating the strong exploratory capabilities of the NSGA-II algorithm in optimizing multiple objectives [36]. The Pareto boundaries emphasize the trade-offs among the objectives, assisting in the selection of optimal solutions for the specific MWC model problem.

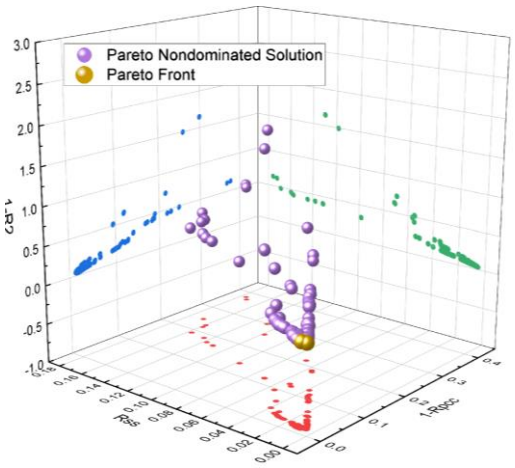

Figure 2 The Pareto nondominated solution and Pareto front

Figure 3 shows the iterative convergence curve, which illustrates that the comprehensive objective function steadily decreases as the number of generations increases. The objective value drops significantly before the 50th generation and then levels off, indicating that the NSGA-II could achieve efficient convergence within a relatively small number of generations.

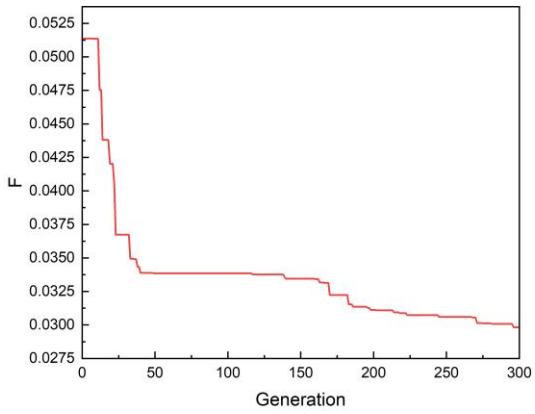

Figure 3 The iterative convergence curve

The results of the Pareto solution set and convergence curve indicate that the optimization algorithm, NSGA-II, exhibits strong computational efficiency and convergence performance when applied to the calculation of Wiebe parameters in the MWC model. It shows a balance between global exploration and local exploitation during the optimization process.

3.1.2 Validation of Results

The final solution for each case is selected from the Pareto nondominated solution set based on the comprehensive objective function. The values of each objective function are presented in Table 5. The error between the fitting results and the experimental data can be assessed from various perspectives using these objective function values. The values of comprehensive objective function F are all below 0.03, indicating a strong fit between the fitting results and the experimental data.

Table 5 The value of objective functions.

Objective function	Case 1	Case 2	Case 3
f_1=min(1-e_{R2})	0.0155	0.0079	0.0091
f_2=min(e_{RSS})	0.0035	0.0020	0.0029
f_3=min(1-e_{PCC})	0.0310	0.0172	0.0184
F=min($\sum w_n f_n$)	0.0267	0.0148	0.0159

Figure 4 to Figure 6 compare the fitting results, simulation results, and experimental data. The results show that during the optimization process, the FBPR of the fitting results and experimental results exhibit a strong correlation. The relative error at key points, such as the maximum FBPR, is below 5%. Additionally, the fitting results follow the same trend as the experimental results.

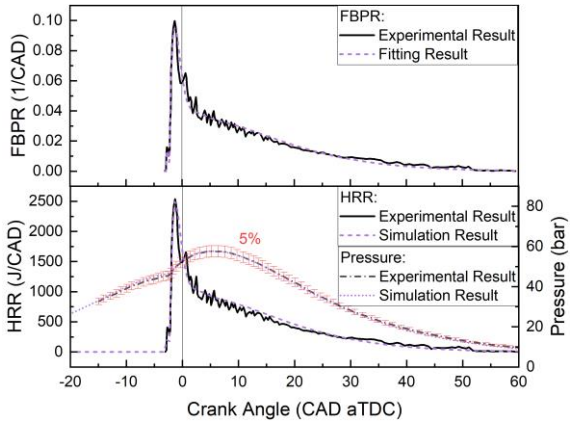

Figure 4 Comparison of FBPR between fitting results and experimental data, as well as a comparison of HRR and pressure between simulation and experimental results, with a diesel SOI of -10 CAD aTDC.

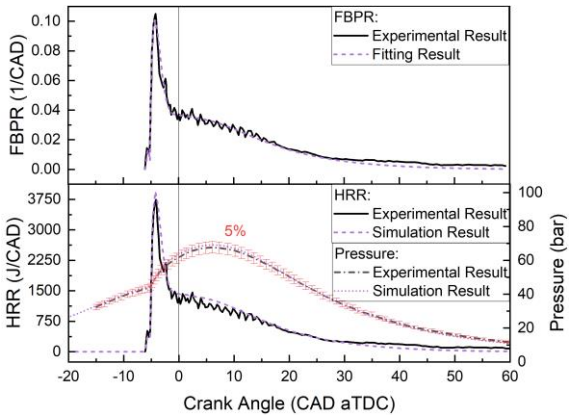

Figure 5 Comparison of FBPR between fitting results and experimental data, as well as a comparison of HRR and pressure between simulation and experimental results, with a diesel SOI of -15 CAD aTDC.

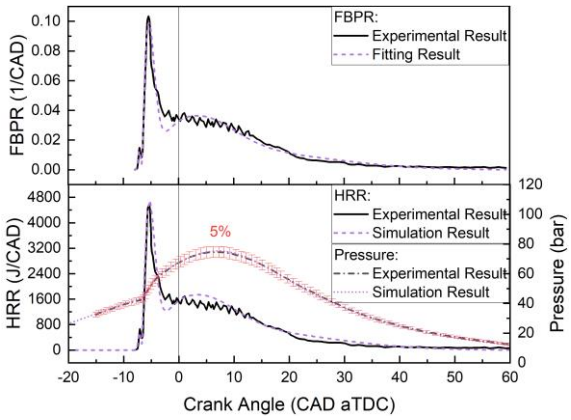

Figure 6 Comparison of FBPR between fitting results and experimental data, as well as a comparison of HRR and pressure between simulation and experimental results, with a diesel SOI of -20 CAD aTDC.

As shown in Figure 4 to Figure 6, when applying the MWC model obtained through optimization to the 1-D simulation model, the Heat Release Rate (HRR) of the simulation results also aligns well with the experimental results, with a relative error of less than 5% at key points and a similar trend. Furthermore, the relative error in in-cylinder pressure between the simulation results and the experimental results is below 5%, demonstrating the high accuracy of both the MWC model and the 1-D simulation model [37].

3.2 Analysis of Fuel Interaction and Its Effect

Through the MWC model, this section mainly analyses the interaction between diesel and ammonia, as well as the impact of diesel injection timing on combustion in the large ADCI engine. Figure 7 presents the Wiebe combustion curves, derived from the Wiebe parameters, showing a

comparison of the FBPR of diesel during the premixed, main, and tail combustion phases under different diesel injection timings. Figure 8 is similar to Figure 7, but focuses especially on ammonia. These two figures will be referenced for the following subsequent analysis in different sections.

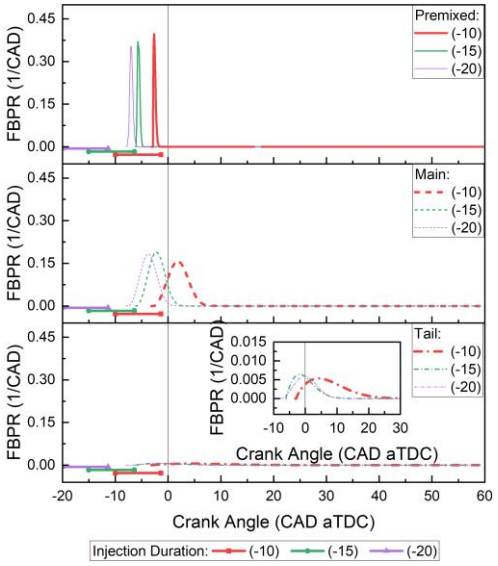

Figure 7 Comparison of the FBPR of diesel across various SOIs during the premixed, main, and tail combustion phases.

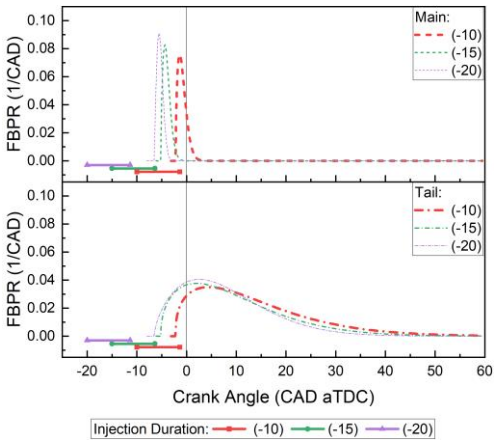

Figure 8 Comparison of the FBPR of ammonia across various SOIs during the premixed, main, and tail combustion phases.

3.2.1 HRR, Pressure and Temperature

Figure 9 illustrates the HRR, in-cylinder pressure and in-cylinder temperature under varying SOI of diesel in the simulation model based on the MWC model. The delayed diesel injection timing results in a lower HRR, driven by the FBPRs shown in Figure 7 and Figure 8. Since the energy share ratio of diesel is less than 10%, and given the premixed ammonia and the small gap between the SoC of diesel and ammonia, the first peak of HRR is mainly determined by the FBPR of both diesel in premixed combustion phase and ammonia in main combustion phase. Based on the FBPRs in the premixed combustion phase, as shown in Figure 7 and Figure 8, although the peak of diesel increases with the delayed diesel injection timing, the lower peak of ammonia has a greater influence on the first peak of HRR due to its higher energy ratio, leading to a lower first peak of HRR, as shown in zone (iii) of Figure 9. As the gap between the SoC of ammonia and diesel narrows with delayed diesel injection timing, the first peak of HRR becomes less significant, as shown in zone (iii) of Figure 9. The second peak of HRR is mainly influenced by the first peak of ammonia, which occurs in the main combustion phase. The lower FBPR in the main combustion phase for ammonia, as shown in Figure 8, results in a lower second peak of HRR, as depicted in Figure 9. Besides, with the delayed diesel injection timing, the lower HRR means reduced heat release, which in turn results in a lower in-cylinder temperature and pressure.

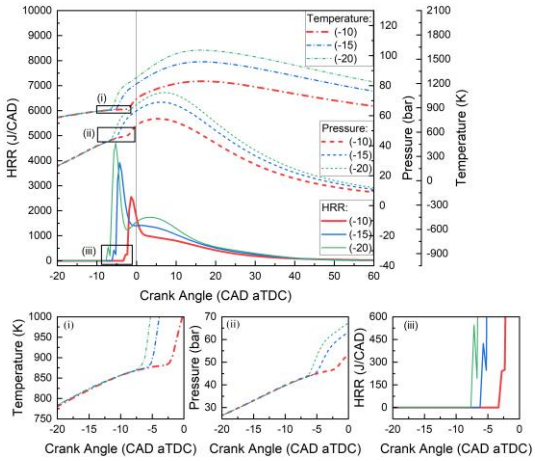

Figure 9 Comparison of the HRR, pressure and temperature across various SOIs.

3.2.2 Ignition and SoC

When the diesel injection timing is delayed from -20 CAD aTDC to -10 CAD aTDC, the diesel is injected into a higher temperature and pressure environment near TDC as shown in zone (i) and zone (ii) of Figure 9. The higher temperature accelerates the evaporation of diesel, while the increased pressure enhances the mixing process between diesel and air, resulting in the formation of a superior diesel-air mixture [38]. Under high-temperature and high-pressure conditions, it is easier to ignite the superior diesel-air mixture, leading to a shorter ignition delay, as shown in Figure 10 [39]. The ignition delay of diesel decreases from 12.46 deg to 7.14 deg, a reduction of 5.32 deg, representing a decrease of up to 42.69%.

In this study, the ignition delay of ammonia is defined as the gap between the SOI of diesel and the SoC of ammonia, as ammonia is premixed and diesel is directly injected. When diesel injection timing is delayed, the higher temperature and pressure also increase the kinetic energy of ammonia, making it easier for ammonia to reach the ignition condition [35]. This results in a reduction of the ignition delay of ammonia from 13.47 deg to 7.8 deg, a decrease of 5.67 deg. The larger reduction in ignition delay of ammonia compared to diesel leads to a smaller gap between the SoC of diesel and ammonia, as shown in Figure 10.

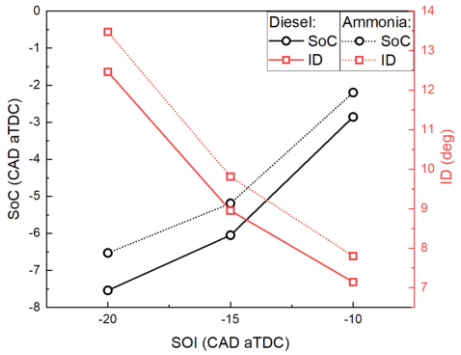

Figure 10 SoC and ID with varying SOI of diesel.

3.2.3 Fuel Burned Proportion

As the diesel injection timing is delayed from -20 CAD aTDC to -10 CAD aTDC, the ignition delay of diesel decreases by up to 42.69%, as mentioned in 3.2.2. The shorter ignition delay reduces the time available for diesel to mix with air before ignition [40]. As shown in Figure 9, when the diesel injection timing is delayed from -20 CAD aTDC to -10 CAD aTDC, the temperature at the SoC of diesel increases from 869 K to 881 K, while the pressure rises from 42 bar to 46 bar. Although higher temperature and pressure can enhance the mixing process [41], the timing of mixing plays a more dominant role, which leads to a decrease in the diesel-air mixture. Since the fuel burned proportion in the premixed combustion phase is primarily determined by the diesel-air mixture before ignition [42], a smaller proportion of diesel is burned in the case of late SOI, as shown in Figure 11.

Since ammonia is premixed with air before entering the cylinder, its combustion primarily consists of two phases. The main combustion phase is driven by in-cylinder temperature and pressure. As ammonia ignition is triggered by diesel, the premixed combustion phase of diesel also influences ammonia combustion. A lower diesel premixed proportion results in reduced heat release during this period, leading to less heat absorption by ammonia for combustion. As shown in Figure 9 and Figure 8, delaying the diesel injection timing lowers the temperature and pressure during ammonia's main combustion phase. This slows the burning rate of ammonia in the main combustion phase, as shown in Figure 8 [43, 44], and reduces the proportion of ammonia burned in the main combustion phase, as shown in Figure 11 [45].

The tail combustion phase of ammonia is defined as the post-combustion period, during which unburned ammonia and other combustion products continue to react. In the tail combustion phase, the proportions of diesel and ammonia burned are determined by the unburned fuel remaining after the main combustion phase [46]. The decreased ammonia burned proportion in the main combustion phase results in more unburned ammonia remaining after the main combustion phase, leading to a lower ammonia burned proportion in the tail combustion phase, as shown in Figure 11. At the same time, the lower diesel burned proportion in the premixed and main combustion phases means a more unburnt diesel remains after the main combustion phase, resulting in a higher diesel burned proportion in the tail combustion phase, as shown in Figure 11.

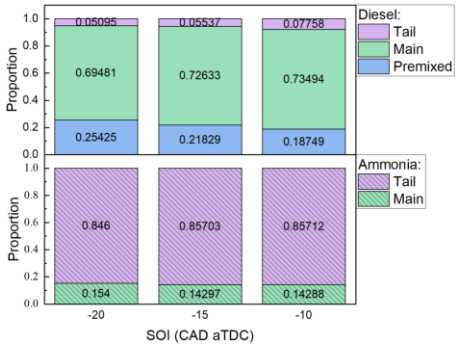

Figure 11 The proportion of fuel burned in different combustion phases with varying SOI of diesel.

3.2.4 Combustion Duration

Figure 12 shows the combustion durations in different combustion phases for both diesel and ammonia. The high energy share ratio of ammonia, at 91.5%, combined with its inherently slower combustion speed than diesel, results in a longer combustion duration for ammonia compared to diesel [47]. As the diesel injection timing is delayed, the combustion duration of both diesel and ammonia increase. This is because the delayed diesel injection timing shifts the SoC closer to TDC, causing the heat to be released primarily during the power stroke rather than the compression stroke. This leads to lower in-cylinder temperature and pressure, as shown in Figure 9 [48]. The lower in-cylinder temperature and pressure result in a slower combustion reaction rate [49]. With further delay in diesel injection timing, a greater portion of

both diesel and ammonia is combusted after TDC, as shown in Figure 7 and Figure 8, leading to a longer combustion duration, as shown in Figure 12.

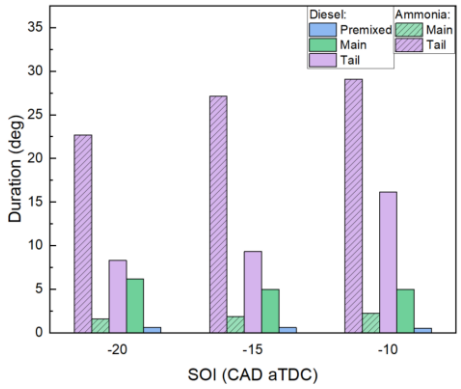

Figure 12 The combustion duration in different combustion phases with varying SOI of diesel.

3.2.5 Combustion Exponent

Combustion exponent defines the shape of the combustion curve and influences the burning rate. As shown in Figure 13, the combustion exponents in different combustion phases for diesel are higher than those of ammonia, indicating that diesel has a faster combustion speed than ammonia [50]. Since diesel is easier to combust than ammonia, this characteristic contributes to its higher combustion quality and speed [51]. In Figure 13, as the diesel injection timing is delayed, the combustion exponents for both diesel and ammonia decrease, indicating an increase in combustion speed.

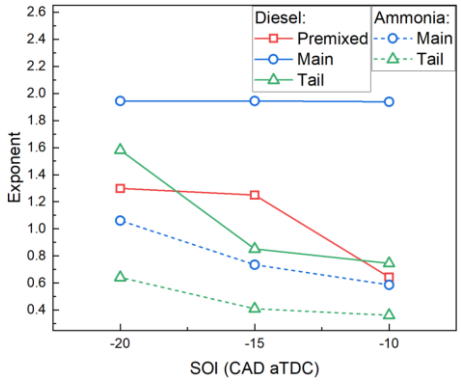

Figure 13 The combustion exponent in different combustion phase with varying SOI of diesel.

3.2.6 Efficiency and ammonia slip

As shown in Figure 14, when the diesel injection timing delayed from -20 CAD aTDC to -10 CAD aTDC, the deterioration in fuel combustion, lower temperature and pressure, results in a decrease in combustion efficiency from 64.86% to 28.2%. It also leads to an increase in ammonia slip from 0.3 to 0.62, normalized by the total ammonia injected into the cylinder [35]. Although delayed diesel injection can shift ignition closer to TDC and increase the percentage of heat released during the power stroke, potentially improving indicated efficiency, the overall reduction in combustion efficiency significantly lowers the peak in-cylinder pressure from 80 to 60 bar, causing the indicated efficiency decreases from 33.79% to 18.33%.

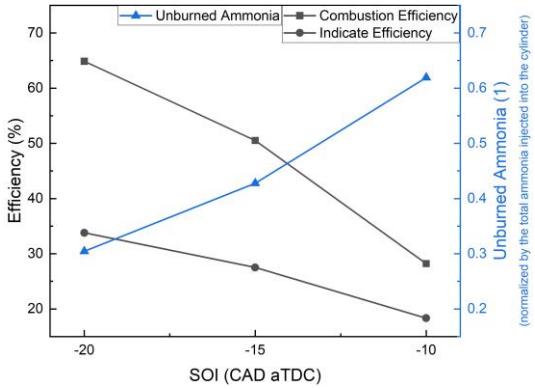

Figure 14 Combustion efficiency, indicate efficiency and unburned ammonia (*Normalized by the total ammonia injected into the cylinder*) under varying SOI of diesel.

4 CONCLUSIONS

This study developed a multi-Wiebe combustion model (MWC) for ammonia-diesel compression ignition (ADCI) engines to enhance the understanding of combustion interactions between ammonia and diesel, while addressing simulation challenges in multi-cylinder ammonia engines. NSGA-II was employed to parameterize and optimize the Wiebe parameters in MWC model. A simulation model in GT-Power was developed to validate the accuracy of the MWC model and support future research at the powertrain level.

The method described above was applied to the study of a special large-bore ADCI engine with premixed ammonia and direct injection of diesel. The results show that the NSGA-II optimization method converges quickly and provides accurate optimization results. It was found that, when the diesel injection timing is delayed, the ignition delay of both ammonia and diesel are shortened, while the premixed combustion of diesel is enhanced and the main combustion of ammonia is weakened. However, the combustion efficiency and indicated efficiency significantly decrease when the diesel injection timing is delayed near TDC, resulting in a high ammonia slip. The high level of ammonia slip indicates that the premixed ammonia engine requires further research to address this issue.

In the next step, it is expected to explore the direct injection of ammonia for marine engines by using the MWC model and NSGA-II developed in this study. This approach will enhance the understanding of the fuel interactions and provide

a simulation model that can be applied at the powertrain level, supporting the advancement and development of ADCI engines.

5 DEFINITIONS, ACRONYMS, ABBREVIATIONS

Nomenclature

English letters

C_{BE}	Burned end constant
C_{BM}	Burned mid-point constant
C_{BS}	Burned start constant
C_{M_a}	Wiebe constant of main combustion phase of ammonia
C_{M_d}	Wiebe constant of main combustion phase of diesel
C_{P_d}	Wiebe constant of premixed combustion phase of diesel
C_{T_a}	Wiebe constant of tail combustion phase of ammonia
C_{T_d}	Wiebe constant of tail combustion phase of diesel
D_{M_a}	Duration of main combustion phase of ammonia, deg
D_{M_d}	Duration of main combustion phase of diesel, deg
D_{P_d}	Duration of premixed combustion phase of diesel, deg
D_{T_a}	Duration of tail combustion phase of ammonia, deg
D_{T_d}	Duration of tail combustion phase of diesel, deg
E_{M_a}	Exponent of main combustion phase of ammonia
E_{M_d}	Exponent of main combustion phase of diesel
e_{PCC}	The value of Pearson Correlation Coefficient
E_{P_d}	Exponent of premixed combustion phase of diesel
e_{R2}	The value of R-squared
e_{RE_rmax}	Relative error of the maximum rate of fuel burned proportion
$e_{RE\_\theta\_rmax}$	Relative error of the crank angle at the maximum rate of fuel burned proportion
e_{RSS}	The value of residual sum of square
E_{T_a}	Exponent of tail combustion phase of ammonia
E_{T_d}	Exponent of tail combustion phase of diesel
F	Comprehensive objective function
G	The number of generations
G_{max}	The maximum thresholds of generations
$InjD_d$	Injection duration of diesel
m_a	Mass of ammonia, kg
m_d	Mass of diesel, kg
N	The number of objective functions
p_a	Proportion of ammonia burned
p_d	Proportion of diesel burned
p_{total}	Proportion of total fuel burned
p_{M_a}	Proportion of ammonia burned in main combustion phase
p_{M_d}	Proportion of diesel burned in main combustion phase
p_{P_d}	Proportion of diesel burned in premixed combustion phase
p_{T_a}	Proportion of ammonia burned in tail combustion phase
p_{T_d}	Proportion of diesel burned in tail combustion phase
p_{total}	Proportion of total fuel burned
P_{M_a}	The integration of the proportion of ammonia burned in main combustion phase
P_{T_a}	The integration of the proportion of ammonia burned in tail combustion phase
r_{exp}	Rate of fuel burned proportion of experimental result
r_{fit}	Rate of fuel burned proportion of fitting result
r_{max_exp}	Maximum rate of fuel burned proportion of experimental result
r_{max_fit}	Maximum rate of fuel burned proportion of fitting result
S_a	Normalized fuel injection rate of ammonia
S_d	Normalized fuel injection rate of diesel
t_{ID_a}	Ignition delay of ammonia, deg
t_{ID_d}	Ignition delay of diesel, deg
$\bar{X}$	The means of variable X
X_i	Individual data point of variable X
$\bar{Y}$	The means of variable Y
Y_i	Individual data point of variable Y

Greek letters

α_a	Fraction of fuel burned or combustion efficiency of ammonia
α_d	Fraction of fuel burned or combustion efficiency of diesel
β_a	Energy share ratio of ammonia
β_d	Energy share ratio of diesel
γ_a	Proportion of ammonia in the mixture
γ_d	Proportion of diesel in the mixture
θ	Instantaneous crank angle, CAD
θ_{SoC_a}	Start of Combustion of

	ammonia, CAD aTDC
θ_{SOI_a}	Start of injection of ammonia, CAD aTDC
θ_{SoC_d}	Start of Combustion of diesel, CAD aTDC
θ_{SOI_d}	Start of injection of diesel, CAD aTDC
θ_{rmax_exp}	Crank angle of experimental result at the maximum rate of fuel burned proportion, CAD
θ_{rmax_fit}	Crank angle of fitting result at the maximum rate of fuel burned proportion, CAD
θ_{EOI_a}	The end of injection point of ammonia, CAD
θ_{EOI_d}	The end of injection point of diesel, CAD
λ_a	Lower heating value of ammonia, MJ/kg
λ_d	Lower heating value of ammonia, MJ/kg
μ_a	Normalized fuel content of ammonia, which has been injected to the cylinder
μ_d	Normalized fuel content of diesel, which has been injected to the cylinder
φ_a	Equivalence ratio of the ammonia/air mixture
ω_n	Weight of the n^{th} objective function f_n
Abbreviations	
0-D	Zero-Dimensional
1-D	One-Dimensional
3-D	Three-Dimensional
ADCI	Ammonia-Diesel Compression Ignition
aTDC	After Top Dead Center
BE	End of Burned
BM	Burned Mid-point
BS	Start of Burned
CAD	Crank Angle Degree
CFD	Computational Fluid Dynamics
CI	Compression Ignition
DI	Direct Injection
EOI	End of Injection
FBPR	Rate of Fuel Burned Proportion
ESR	Energy Share Ratio
HRR	Heat Release Rate
ID	Ignition Delay
MCP	Main Combustion Phase
MWC	Multi-Wiebe Combustion
NSGA-II	Non-dominated Sorting Genetic Algorithm II
PCC	Pearson Correlation Coefficient
PCP	Premixed Combustion Phase
PFI	Port Fuel Injection
R^2	R-squared
RE	Relative Error
RSS	Residual Sum of Squares
SoC	Start of Combustion
SOI	Start of Injection
TCP	Tail Combustion Phase
TDC	Top Dead Center

6 ACKNOWLEDGMENTS

This work was supported by EPSRC (Engineering and Physical Sciences Research Council, United Kingdom) (Grant numbers: EP/W016656/1, EP/Y024605/1), and the authors would also like to thank the support from China Scholarship Council for the Stipend Scholarship awarded to the first author.

7 REFERENCES AND BIBLIOGRAPHY

[1] I. E. A. (IEA) 2023. Energy and Carbon Tracker.

[2] S. Joseph Sekhar, A. Said Ahmed Al-Shahri, G. Glivin, T. H. T. Le, and T. Mathimani, 2024. A critical review of the state-of-the-art green ammonia production technologies- mechanism, advancement, challenges, and future potential, (in English), *Fuel,* Article vol. 358, 130307, doi: 10.1016/j.fuel.2023.130307.

[3] S. Sun *et al.*, 2022. Ammonia as hydrogen carrier: Advances in ammonia decomposition catalysts for promising hydrogen production, (in English), *Renewable Sustainable Energy Rev,* Review vol. 169, 112918, doi: 10.1016/j.rser.2022.112918.

[4] C. Kurien and M. Mittal, 2022. Review on the production and utilization of green ammonia as an alternate fuel in dual-fuel compression ignition engines, (in English), *Energy Conversion and Management,* Review vol. 251, 114990, doi: 10.1016/j.enconman.2021.114990.

[5] K. O. P. Bjørgen, D. R. Emberson, and T. Løvås, 2024. Combustion of liquid ammonia and diesel in a compression ignition engine operated in high-pressure dual fuel mode, *Fuel,* Article vol. 360, 130269, doi: 10.1016/j.fuel.2023.130269.

[6] S. Jin, B. Wu, Z. Zi, P. Yang, T. Shi, and J. Zhang, 2023. Effects of fuel injection strategy and ammonia energy ratio on combustion and emissions of ammonia-diesel dual-fuel engine, *Fuel,* Article vol. 341, 127668, doi: 10.1016/j.fuel.2023.127668.

[7] E. Nadimi, G. Przybyła, M. T. Lewandowski, and W. Adamczyk, 2023. Effects of ammonia on combustion,

emissions, and performance of the ammonia/diesel dual-fuel compression ignition engine, *Journal of the Energy Institute,* Article vol. 107, 101158, doi: 10.1016/j.joei.2022.101158.

[8] A. Hossein Fakhari, A. Gharehghani, M. Mahdi Salahi, and A. Mahmoudzadeh Andwari, 2024. RCCI combustion of ammonia in dual fuel engine with early injection of diesel fuel, *Fuel,* Article vol. 365, 131182, doi: 10.1016/j.fuel.2024.131182.

[9] A. M. Elbanna and X. Cheng, 2024. The role of charge reactivity in ammonia/diesel dual fuel combustion in compression ignition engine, (in English), *Energy,* Article vol. 306, 132387, doi: 10.1016/j.energy.2024.132387.

[10] J. Shin and S. Park, 2024. Numerical analysis and optimization of combustion and emissions in an ammonia-diesel dual-fuel engine using an ammonia direct injection strategy, *Energy,* Article vol. 289, 130014, doi: 10.1016/j.energy.2023.130014.

[11] X. Wang *et al.*, 2024. Experimental investigation on in-cylinder working process and thermal efficiency of ammonia/diesel low-carbon engine with pre-injection strategy, *Appl Therm Eng,* Article vol. 248, 123272, doi: 10.1016/j.applthermaleng.2024.123272.

[12] J. Liu, X. Wang, W. Zhao, P. Sun, and Q. Ji, 2024. Effects of ammonia energy fraction and diesel injection parameters on combustion stability and GHG emissions characteristics in a low-loaded ammonia/diesel dual-fuel engine, *Fuel,* Article vol. 360, 130544, doi: 10.1016/j.fuel.2023.130544.

[13] T. Li *et al.*, 2022. A comparison between low- and high-pressure injection dual-fuel modes of diesel-pilot-ignition ammonia combustion engines, *Journal of the Energy Institute,* Article vol. 102, pp. 362-373, Art no., doi: 10.1016/j.joei.2022.04.009.

[14] K. Kishore, C. Kurien, and M. Mittal, 2024. Experimental and numerical analysis of engine characteristics of an ammonia-substituted dual-fuel CRDI diesel engine, *Fuel,* Article vol. 366, 131354, doi: 10.1016/j.fuel.2024.131354.

[15] N. N. Yao, Y. F. Chen, L. M. Wei, Q. Y. Xu, and W. G. Pan, 2025. Progress in CFD simulation for ammonia-fueled internal combustion engines and gas turbines, (in English), *Journal of the Energy Institute,* Review vol. 119, 101951, doi: 10.1016/j.joei.2024.101951.

[16] K. Kuta, E. Nadimi, G. Przybyła, Z. Żmudka, and W. Adamczyk, 2022. Ammonia ci engine aftertreatment systems design and flow simulation, *Combustion Engines,* Article vol. 190, no. 3, pp. 3-10, Art no., doi: 10.19206/CE-143158.

[17] T. Oppl, G. Pirker, M. Wohlthan, and A. Wimmer, 2022. Development of a zero-dimensional method for thermodynamic analysis and NOx calculation in the prechamber of a lean-burn gas engine, (in English), *International Journal of Engine Research,* Article vol. 23, no. 11, pp. 1850-1863, Art no., doi: 10.1177/14680874211037845.

[18] J. Galindo, H. Climent, B. Plá, and V. D. Jiménez, 2011. Correlations for Wiebe function parameters for combustion simulation in two-stroke small engines, (in English), *Appl Therm Eng,* Article vol. 31, no. 6-7, pp. 1190-1199, Art no., doi: 10.1016/j.applthermaleng.2010.12.020.

[19] B. Rajendra Prasath, P. Tamilporai, and M. F. Shabir, 2010. Analysis of combustion, performance and emission characteristics of low heat rejection engine using biodiesel, (in English), *Int. J. Therm. Sci.,* Article vol. 49, no. 12, pp. 2483-2490, Art no., doi: 10.1016/j.ijthermalsci.2010.07.010.

[20] J. Kim, C. Bae, and G. Kim, 2013. Simulation on the effect of the combustion parameters on the piston dynamics and engine performance using the Wiebe function in a free piston engine, (in English), *Applied Energy,* Article vol. 107, pp. 446-455, Art no., doi: 10.1016/j.apenergy.2013.02.056.

[21] F. Maroteaux and C. Saad, 2013. Diesel engine combustion modeling for hardware in the loop applications: Effects of ignition delay time model, (in English), *Energy,* Article vol. 57, pp. 641-652, Art no., doi: 10.1016/j.energy.2013.03.098.

[22] F. Maroteaux and C. Saad, 2015. Combined mean value engine model and crank angle resolved in-cylinder modeling with NOx emissions model for real-time Diesel engine simulations at high engine speed, (in English), *Energy,* Article vol. 88, pp. 515-527, Art no., doi: 10.1016/j.energy.2015.05.072.

[23] C. V. Ngayihi Abbe, R. Nzengwa, R. Danwe, Z. M. Ayissi, and M. Obonou, 2015. A study on the 0D phenomenological model for diesel engine simulation: Application to combustion of Neem methyl esther biodiesel, (in English), *Energy Conversion and Management,* Article vol. 89, pp. 568-576, Art no., doi: 10.1016/j.enconman.2014.10.005.

[24] O. Bondarenko and T. Fukuda, 2020. Development of a diesel engine's digital twin for predicting propulsion system dynamics, (in English), *Energy,* Article vol. 196, 117126, doi: 10.1016/j.energy.2020.117126.

[25] M. M. N. de Faria, J. P. Vargas Machuca Bueno, S. M. M. E. Ayad, and C. R. P. Belchior, 2017. Thermodynamic simulation model for predicting the performance of spark ignition engines using biogas as fuel, (in English), *Energy Conversion and Management,* Article vol. 149, pp. 1096-1108, Art no., doi: 10.1016/j.enconman.2017.06.045.

[26] H. Sapra, M. Godjevac, P. De Vos, W. Van Sluijs, Y. Linden, and K. Visser, 2020. Hydrogen-natural gas combustion in a marine lean-burn SI engine: A comparitive analysis of Seiliger and double Wiebe function-based zero–dimensional modelling, (in English), *Energy Conversion and Management,* Article vol. 207, 112494, doi: 10.1016/j.enconman.2020.112494.

[27] F. Z. Aklouche, K. Loubar, A. Bentebbiche, S. Awad, and M. Tazerout, 2018. Predictive model of the diesel engine operating in dual-fuel mode fuelled with different gaseous fuels, (in English), *Fuel,* Article vol. 220, pp. 599-606, Art no., doi: 10.1016/j.fuel.2018.02.053.

[28] L. Tipanluisa, K. Thakkar, N. Fonseca, and J. M. López, 2022. Investigation of diesel/n-butanol blends as drop-in fuel for heavy-duty diesel engines: Combustion, performance, and emissions, (in English), *Energy Conversion and Management,* Article vol. 255, 115334, doi: 10.1016/j.enconman.2022.115334.

[29] J. Liu and C. E. Dumitrescu, 2020. Investigation of Multistage Combustion Inside a Heavy-Duty Natural-Gas Spark-Ignition Engine Using Three-Dimensional Computational Fluid Dynamics Simulations and the Wiebe-Function Combustion Model, (in English), *Journal of Engineering for Gas Turbines and Power,* Article vol. 142, no. 10, 101012, doi: 10.1115/1.4045869.

[30] S. Loganathan, M. Leenus Jesu Martin, B. Nagalingam, and L. Prabhu, 2018. Heat release rate and performance simulation of DME fuelled diesel engine using oxygenate correction factor and load correction factor in double Wiebe function, (in English), *Energy,* Article vol. 150, pp. 77-91, Art no., doi: 10.1016/j.energy.2018.02.112.

[31] B. L. Salvi and K. A. Subramanian, 2022. A novel approach for experimental study and numerical modeling of combustion characteristics of a hydrogen fuelled spark ignition engine, (in English), *Sustainable Energy Technologies and Assessments,* Article vol. 51, 101972, doi: 10.1016/j.seta.2022.101972.

[32] C. Mishra and P. M. V. Subbarao, 2021. Design, development and testing a hybrid control model for RCCI engine using double Wiebe function and random forest machine learning, (in English), *Control Engineering Practice,* Article vol. 113, 104857, doi: 10.1016/j.conengprac.2021.104857.

[33] J. Zhu *et al.*, 2022. Development and Validation of a Modeling and Calibration Method for Diesel-Like Multistage Combustion Based On a Modified Multi-Wiebe Function, (in English), *ACS Omega,* Article vol. 7, no. 14, pp. 11756-11769, Art no., doi: 10.1021/acsomega.1c06858.

[34] R. Yang, Z. Ran, and D. Assanis, 2023. Estimation of Wiebe Function Parameters for Syngas and Anode Off-Gas Combustion in Spark-Ignition Engines, (in English), *Journal of Engineering for Gas Turbines and Power,* Article vol. 145, no. 6, 071004, doi: 10.1115/1.4056856.

[35] L. Xu, S. Xu, X. S. Bai, J. A. Repo, S. Hautala, and J. Hyvönen, 2023. Performance and emission characteristics of an ammonia/diesel dual-fuel marine engine, (in English), *Renewable Sustainable Energy Rev,* Article vol. 185, 113631, doi: 10.1016/j.rser.2023.113631.

[36] K. Deb, S. Agrawal, A. Pratap, and T. Meyarivan, 2000. A fast elitist non-dominated sorting genetic algorithm for multi-objective optimization: NSGA-II, (in English), *Lect. Notes Comput. Sci.,* Article vol. 1917, pp. 849-858, Art no., doi: 10.1007/3-540-45356-3_83.

[37] M. Walter, M. Storch, and S. Wartzack, 2014. On uncertainties in simulations in engineering design: A statistical tolerance analysis application, (in English), *Simulation,* Article vol. 90, no. 5, pp. 547-559, Art no., doi: 10.1177/0037549714529834.

[38] A. Deep, S. S. Sandhu, and S. Chander, 2017. Experimental investigations on the influence of fuel injection timing and pressure on single cylinder C.I. engine fueled with 20% blend of castor biodiesel in diesel, (in English), *Fuel,* Article vol. 210, pp. 15-22, Art no., doi: 10.1016/j.fuel.2017.08.023.

[39] M. K. Bobba, C. L. Genzale, and M. P. Musculus, 2009. Effect of ignition delay on in-cylinder soot characteristics of a heavy duty diesel engine operating at low temperature conditions, *SAE International Journal of Engines,* vol. 2, no. 1, pp. 911-924, Art no.

[40] S. Rabl, T. Davies, A. McDougall, and R. Cracknell, 2015. Understanding the relationship between ignition delay and burn duration in a constant volume vessel at diesel engine conditions, *Proceedings of the Combustion Institute,* vol. 35, no. 3, pp. 2967-2974, Art no.

[41] J. Ismatov, J. Khakimov, S. Eshkabilov, and N. Vadulina, 2021. Processes of mixture formation, ignition and combustion of a diesel engine, *Annals of the Romanian Society for Cell Biology,* pp. 6527-6545, Art no.

[42] Y. H. Teoh *et al.*, 2021. Effect of intake air temperature and premixed ratio on combustion and exhaust emissions in a partial HCCI-DI diesel engine, (in English), *Sustainability (Switzerland),* Article vol. 13, no. 15, 8593, doi: 10.3390/su13158593.

[43] A. Yousefi, H. Guo, S. Dev, B. Liko, and S. Lafrance, 2022. Effects of ammonia energy fraction and diesel injection timing on combustion and emissions of an ammonia/diesel dual-fuel engine, *Fuel,* vol. 314, p. 122723, Art no.

[44] C. Yang, Z. Wang, J. Li, and X. Cheng, 2024. Effects of ammonia energy fractions, diesel injection timings, and loads on combustion and emission characteristics of PFI-DI ammonia-diesel engines, *International Journal of Engine Research,* vol. 25, no. 4, pp. 743-757, Art no.

[45] X. Gao *et al.*, 2024. The Influence of Injection Strategy on the Ignition Characteristics of Diesel/Ammonia Premixture, (in English), *Fluids,* Article vol. 9, no. 10, 224, doi: 10.3390/fluids9100224.

[46] W. Sun *et al.*, 2023. An optical study of the combustion and flame development of ammonia-diesel dual-fuel engine based on flame chemiluminescence, *Fuel,* vol. 349, p. 128507, Art no.

[47] J. Frost, A. Tall, A. M. Sheriff, A. Schönborn, and P. Hellier, 2021. An experimental and modelling study of dual fuel aqueous ammonia and diesel combustion in a single cylinder compression ignition engine, (in English), *International Journal of Hydrogen Energy,* Article vol. 46, no. 71, pp. 35495-35510, Art no., doi: 10.1016/j.ijhydene.2021.08.089.

[48] S. Rostami, B. Ghobadian, and M. K. D. Kiani, 2014. Effect of the injection timing on the performance of a diesel engine using Diesel-Biodiesel blends, *International Journal of Automotive and Mechanical Engineering,* vol. 10, pp. 1945-1958, Art no.

[49] J. Agboola, B. T. Lebele-Alawa, and B. Nkoi, 2018. A Study Of Combustion Temperature Distribution In The Cylinder Of Compression Ignition Engine, *American Journal of Engineering Research,* vol. 7, no. 11, pp. 304-312, Art no.

[50] J. Famfulik, M. Richtar, J. Smiraus, P. Muckova, B. Sarkan, and P. Dresler, 2021. Internal combustion engine diagnostics using statistically processed wiebe function, (in English), *Eksploatacja Niezawodnosc,* Article vol. 23, no. 3, pp. 505-511, Art no., doi: 10.17531/ein.2021.3.11.

[51] H. Xiao *et al.*, 2024. Study on the Impact of Ammonia–Diesel Dual-Fuel Combustion on Performance of a Medium-Speed Diesel Engine, *Journal of Marine Science and Engineering,* vol. 12, no. 5, p. 806, Art no.